Progress In Electromagnetics Research M, Vol. 102, 91–104, 2021

A Hybrid Inversion Method Based on the Bat Algorithm for Microwave Imaging of Two-Dimensional Dielectric Scatterers

Chun Xia Yang[1, *], Jian Zhang[2], and Mei Song Tong[2]

Abstract—In this article, a hybrid inversion method based on the bat algorithm (BA) is proposed. Electromagnetic inverse scattering problems are ill-posed and are often transformed into optimization problems by defining a suitable cost function. As typical methods to solve optimization problems, stochastic optimization algorithms are more flexible and have better global searching ability than deterministic algorithms. However, they share a common disadvantage: heavy computing load. This directly restricts the application of the algorithms in high-dimensional problems and real-time imaging environments. To solve this issue, diffraction tomography (DT) is introduced to provide a reference for the initialization of the BA. Furthermore, the hybrid method makes full use of the complementary advantages of linear reconstruction algorithms and stochastic optimization algorithms to improve accuracy and efficiency at the same time. Moreover, in order to avoid the algorithm falling into local extrema, an attenuation strategy of the pulse emission rate is proposed to enable more bats to perform global search in the early stage of the algorithm. In the numerical experiments for different types of dielectric objects, the reconstruction results of this hybrid BA-based algorithm are compared with those of the DT and particle swarm optimization (PSO).

1. INTRODUCTION

Electromagnetic inverse scattering refers to the process of using electromagnetic waves to illuminate the imaging region and then estimating the distribution of scatterers according to the echo information [1, 2]. As a non-contact imaging model, it has been widely used in medical diagnostics [3–6], nondestructive testing [7], geophysical applications, buried object detection [8–11], etc. [12, 13]. However, the inverse scattering problem is much more complex than the forward one. It is nonlinear due to the multiple scattering phenomenon, which indicates that the scattered field formed by two scatterers is not equal to the linear superposition of the scattered field formed by each of the scatterers [14]. Furthermore, the limitation of the frequency spectrum makes the solution of the inverse problem non-unique [15, 16]. The reconstructed image is a low-pass filtered version of the original object [17]. If the object has some fine structures which are small compared to the wavelength of the incident wave, local evanescent wave will be formed. The evanescent wave is oscillating electromagnetic field that does not propagate and is thus difficult to capture outside the imaging domain. Therefore, the exploration of efficient electromagnetic inversion methods has been an important research direction in computational electromagnetics. Especially in recent years, the rapid development of large-scale computing machines and parallel computing technologies made it possible to solve complex inverse scattering problems and realize many novel inversion algorithms.

Due to the ill-posedness of inverse scattering problems, they are often transformed into optimization problems [18–20]. Generally, optimization methods can be divided into deterministic ones and stochastic

Received 28 January 2021, Accepted 3 April 2021, Scheduled 16 April 2021
* Corresponding author: Chunxia Yang (chunxia@illinois.edu).
[1] Shanghai Engineering Research Center of Intelligent Education and Bigdata, Shanghai Normal University, Shanghai 200234, China.
[2] Shanghai Institute of Intelligent Science and Technology, Tongji University, Shanghai 201203, China.

ones. The optimization process of deterministic algorithms relies on the gradient information of the cost function [21, 22]. So, when the initial solution and the number of iterations are determined, the final solution will always be the same no matter how many times the algorithm is repeated. With the help of the gradient, deterministic algorithms could achieve high efficiency, and the optimal solution can be obtained after a few iterations [23–25]. However, with the wide application of inverse scattering in engineering, complex models and imaging environments make the problem even more challenging. The overdependence on gradient may cause deterministic algorithms to fall into local extrema and yield false solutions.

The use of stochastic optimization algorithms could alleviate this problem. The introduction of random factors enables the algorithms to jump out of the attractive domain of local extrema [26]. Moreover, compared with deterministic algorithms, stochastic optimization algorithms have two significant advantages. First, in the implementation of stochastic optimization algorithms, one does not need to analyze the cost function. And the complicated mathematical derivation can be avoided. Second, stochastic optimization algorithms are more flexible. By adjusting the control parameters and imposing restrictions, they can make full use of the *a priori* information to avoid yielding invalid solutions [27]. The application bottleneck of stochastic optimization algorithms is that global search may bring heavy computing load. Fortunately, the efficiency of the algorithm can be improved by virtue of its inherent parallelism.

The first stochastic optimization algorithm applied to electromagnetic inverse scattering problems was genetic algorithm (GA) [28]. The GA simulates the evolution process of organisms by performing the selection, crossover, and mutation operations. Subsequently, the differential evolution algorithm (DE) [29] and PSO [30–32] were also introduced to microwave imaging. The PSO simulates the foraging behavior of birds. Individuals in the population communicate and collaborate during the search process and eventually gather near the food source. The PSO is characterized by the particle's ability to remember and learn from other individuals. The imitation of biological evolution or foraging behavior gives such algorithms some natural intelligence. This is why they are also called heuristic algorithms.

In recent years, a new nature-inspired optimization algorithm, the bat algorithm (BA), attracted attentions from many researchers. The BA was proposed by Yang et al. in 2010 [33]. It imitates the foraging behavior of microbats and exploits their echolocation ability. Similar to the PSO, each location of the individual represents a possible solution to the problem. The main control parameters in the BA include pulse emission rate, frequency, and loudness. The most significant difference between the BA and other heuristic algorithms is that individuals only move to positions that are better than their current ones [34, 35]. Another difference is that the BA has two iterating approaches: global search and local search [36]. Bats performing the local search will search for a new random location near the current optimal solution [37]. The BA has been successfully applied to many practical engineering problems [38, 39], but the research in the field of microwave imaging is still immature. In this paper, we reconstruct dielectric objects with a hybrid BA-based inversion algorithm.

In this paper, two modifications to the standard BA are proposed to improve the performance and make it applicable in microwave imaging problems. First, a decreasing strategy of the pulse emission rate is adopted to improve the global search ability of the algorithm at the early stage of optimization. Second, a hybrid inversion strategy is designed. The reconstruction result of DT is taken as an initial trial solution of the BA. This trial solution provides guidance for the individual initialization of the stochastic optimization algorithm so that optimal results can be achieved with fewer iterations.

The paper is organized as follows. The imaging model and related formulas of a 2-D electromagnetic inverse scattering problem will be given in Section 2. The cost function including the regularization term will also be defined here. The steps of the BA and its customized improvements are described in Section 3. The flowchart of the hybrid inversion algorithm is also given in this section. In Section 4, several numerical examples for imaging typical objects in 2-D are presented to illustrate the proposed approach, and good imaging results can be observed.

2. MICROWAVE IMAGING PROBLEM

Consider a microwave imaging model as shown in Fig. 1. The imaging domain D_i is defined in the free space with a permittivity ε_0 and a permeability μ_0. An unknown dielectric object is enclosed in the

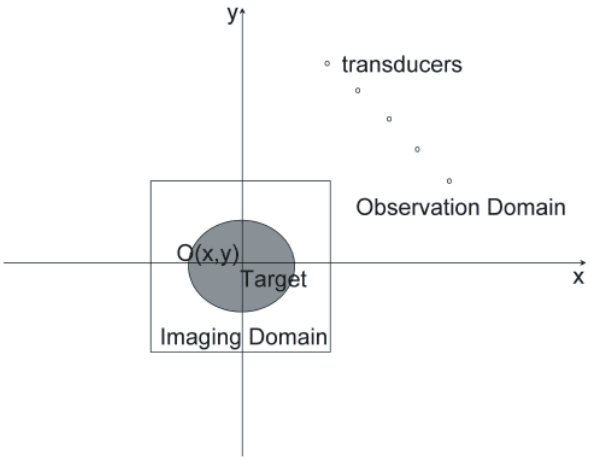

Figure 1. Microwave imaging model.

imaging domain. The permittivity and permeability of the object are $\varepsilon(x, y)$ and $\mu(x, y)$, respectively. Microwave imaging is a non-contact method, which means that the transmitting and receiving stations of electromagnetic waves are arranged in the observation domain D_o outside the imaging domain. Here, we consider a 2-D inversion problem and use totally V incident TMz waves to illuminate the imaging domain successively. Electric current is induced on the unknown object, generating scattered field which is received by the observation stations.

The governing equations of this electromagnetic inverse scattering problem are the following electric field integral equations [14]:

$$\begin{aligned} E^{sca}(x,y) &= E^{tot}(x,y) - E^{inc}(x,y) \\ &= k_0^2 \int_{D_i} g(x,y;x',y') \cdot O(x',y') E^{tot}(x',y')\, dx'dy', \quad (x,y) \in D_o, \end{aligned} \tag{1}$$

and

$$\begin{aligned} E^{tot}(x,y) &= E^{inc}(x,y) \\ &\quad + k_0^2 \int_{D_i} g(x,y;x',y') \cdot O(x',y') E^{tot}(x',y')\, dx'dy', \quad (x,y) \in D_i, \end{aligned} \tag{2}$$

where $E_z^{sca}(x,y)$, $E_z^{tot}(x,y)$, and $E_z^{inc}(x,y)$ denote the scattered field, total field, and incident field, respectively. Coordinates (x, y) and (x', y') denote the field point and source point, respectively.

In Eq. (1), $g(x,y;x',y') = \frac{i}{4} H_0^{(1)}(k_0\sqrt{(x-x')^2+(y-y')^2})$ is the 2-D Green's function in the free space, and $H_0^{(1)}$ is the zero-order Hankel function of the first kind. k_0 is the wave number in the background. Here, the contrast that indicates the unknown scatterer is related to the distribution of the relative permittivity $O(x,y) = \varepsilon_r(x,y) - 1$ because the object is assumed to be non-magnetic.

To transform the continuous equations into discrete ones, we divide the imaging domain into N cells and use rectangular basis function to expand the contrast, yielding $O(x,y) = \sum_{n=1}^{N} a_n b_n(x,y)$. In this discretization scheme, the contrast within each cell is assumed to be constant.

The inverse scattering integral equation cannot be solved directly because it is ill-posed. One approach is to transform it into an optimization problem by adding a regularization term. Define the following cost function [14]:

$$\begin{aligned} C(a_n) &= \delta \sum_{n,m} a_n a_m^* \int_{D_i} b_n(x',y') b_m^*(x',y')\, dx'dy' + \sum_v \sum_{(x,y)\in D_o} \Bigg| E_v^{sca}(x,y) \\ &\quad - k_0^2 \sum_n a_n \int_{D_i} g(x,y;x',y') \cdot b_n(x',y') E_v^{tot}(x',y')\, dx'dy' \Bigg|^2. \end{aligned} \tag{3}$$

The first term on the right hand side is the regularization term, which corresponds to the norm of the contrast. This could help avoid getting multiple solutions. The second term is the error between the measured scattered field data and the predicted or calculated data. It consists of contributions from totally V incident fields. δ is a regularization parameter and works to adjust the weight of the two terms in this optimization model. With the defined cost function, the inverse scattering problem is recast as the optimization for coefficients a_n.

3. APPLICATION OF THE BAT ALGORITHM

The BA is a multi-agent optimization algorithm that simulates the foraging behavior of bats. In the BA, bats fly around in the multi-dimensional solution space and adjust their positions according to certain rules. Unlike other stochastic optimization algorithms, the BA takes inspiration from the echolocation ability of bats and adjusts the individuals' flight states through control parameters including frequency, loudness, and pulse emission rate. Note that the frequency as a control parameter is not related to the frequency of electromagnetic wave. The major steps of the BA and the improvements made in this paper can be summarized as follows.

3.1. Initialization

Set the iteration counter to $t = 0$. Set the population size P, the maximum number of iterations K (or some other iteration termination conditions), and the frequency range $[f_{\min}, f_{\max}]$. Then a swarm of P bats is initialized by randomly generating the associated locations $\{\mathbf{x}_i(t)|i = 1, 2, \ldots, P,\ t = 0\}$ and velocities $\{\mathbf{v}_i(t)|i = 1, 2, \ldots, P,\ t = 0\}$ within the specified ranges $[x_{\min}, x_{\max}]$ and $[v_{\min}, v_{\max}]$, respectively. Initialize the loudness $\{A_i(t)|i = 1, 2, \ldots, P,\ t = 0\}$ and the pulse emission rate $\{r_i(t)|i = 1, 2, \ldots, P,\ t = 0\}$ for the bats.

These control parameters are selected based on the *a priori* information of the inverse problem. The parameters bring two advantages to stochastic optimization algorithms. One is flexibility. The search direction and step size of each individual can be adjusted by control parameters. The deterministic algorithms, however, are entirely dependent on the gradient of the cost function. Another advantage is the ability to impose constraints. Appropriate constraints can prevent the algorithm from yielding false solutions that have no physical meanings or do not meet the specific requirements of the problem. In this paper, we only specify the upper and lower limits of position, which correspond to the value range of contrast in the inverse scattering problem. Actually, more information about scatterers such as number, shape, and central point can be added to stochastic optimization algorithms as constraints. This also helps to narrow the solution space.

Next, the fitness of each bat is evaluated by the cost function in Eq. (3). Then the best fitness value and its corresponding position are marked as $fbest$ and $\mathbf{p}^*$, respectively. In subsequent iterations, new fitness values are calculated and compared to update $fbest$ and $\mathbf{p}^*$. It is ensured that they always represent the best fitness value and position achieved by the population.

3.2. Position Updating

The BA has two search modes: global search and local search. In each iteration, based on a certain probability, each bat randomly chooses to search within a global range or a local range. This probability is determined by the pulse emission rate and is independent of other individuals. To be specific, at moment t, a random variable $rand_1 \in (0, 1)$ is drawn from a uniform distribution. If $rand_1 < r_i(t)$, then the ith bat performs global searching. Otherwise, it searches locally.

The iterating formula of global search can be represented as

$$\mathbf{x}_i'(t+1) = \mathbf{x}_i(t) + \mathbf{v}_i(t+1), \tag{4}$$

and the velocity updating equation at moment $t + 1$ can be written as

$$\mathbf{v}_i(t+1) = \mathbf{v}_i(t) + (\mathbf{x}_i(t) - \mathbf{p}^*) \cdot f_i(t), \tag{5}$$

where the frequency $f_i(t)$ is a random number within $[f_{\min}, f_{\max}]$. The second term of the above equation shows that the bat is trying to move away from the current best position $\mathbf{p}^*$. That's why this update mode is called global search. The higher the frequency is, the farther the bat tries to fly away from $\mathbf{p}^*$.

The local search does not depend on velocity. In this mode, the bat's position is updated according to the following equation.

$$\mathbf{x}_i'(t+1) = \mathbf{p}^* + rand_2 \cdot \bar{A}(t), \tag{6}$$

where $rand_2$ is randomly drawn from a uniform distribution within $(-1, 1)$, and $\bar{A}(t) = \sum_{i=1}^{P} A_i(t)/P$ represents the average loudness of all bats at moment t. Obviously, bats in local search mode wander around the current best location.

Notice that the bat position of the new generation in the above equations is expressed as $\mathbf{x}_i'(t+1)$, not $\mathbf{x}_i(t+1)$. That is because the bat still needs to decide whether to move to this new location. Only when the following two conditions are met does the bat move to $\mathbf{x}_i'(t+1)$; otherwise, the bat will remain at $\mathbf{x}_i(t)$. First, the fitness corresponding to $\mathbf{x}_i'(t+1)$ is better than that of $\mathbf{x}_i(t)$, i.e., $C(\mathbf{x}_i'(t+1)) < C(\mathbf{x}_i(t))$. Second, $rand_3 < A_i(t)$, where $rand_3 \in (0, 1)$ is an uniformly distributed random number.

3.3. Loudness and Pulse Emission Rate Updating

In the standard BA, the loudness decreases, and the pulse emission rate increases as the iterations proceed. In the $t+1$th iteration, if the bat moves to a new position, its loudness and pulse emission rate are updated to

$$A_i(t+1) = \alpha A_i(t), \tag{7}$$

and

$$r_i(t+1) = r_i(0) \cdot \left(1 - e^{-\gamma t}\right), \tag{8}$$

where α and γ are constant parameters. Equation (6) shows that loudness affects the local search scope of bats. As the bat approaches the prey, loudness decreases. And α is similar to the cooling factor in the simulated annealing algorithm. The rate of pulse can simply be in the range of $[0, 1]$, where 0 means no pulse, and 1 indicates the maximum pulse emission rate.

3.4. Improvements to the Standard BA

One of the proposed improvements is the attenuation strategy of the pulse emission rate. The pulse emission rate determines the probability, based on which bats choose to perform global or local searches. The higher the pulse emission rate is, the greater the probability that bats perform global searches is. In Equation (8), the pulse emission rate increases exponentially to $r_i(0)$. Numerical simulations show that the pulse emission rate is too low to provide effective global search in the early stage of the algorithm when it is applied to inverse scattering problems. Therefore, here we propose an attenuation strategy to control the variation of the pulse emission rate.

$$r_i(t+1) = \xi r_i(t) \tag{9}$$

where $\xi \in (0, 1)$ is a constant parameter. This improvement allows more bats to perform global searches in the early stages of the algorithm, avoiding the algorithm falling into local extrema.

Computational efficiency is the bottleneck that blocks the application of stochastic optimization algorithms in electromagnetic inverse problems. In order to improve the efficiency for solving inverse problems, a linear inversion algorithm is introduced to form a hybrid electromagnetic inversion algorithm together with the BA. The result of DT is used as one of the initial trial solutions of the subsequent stochastic optimization. Microwave DT is a linearized electromagnetic inversion technology based on the Born approximation. It establishes a relationship between the scattered field and the electromagnetic properties of the scatterer through Fourier transform. Compared with the randomly generated trial solutions, the DT result is closer to the optimal location. So, the imaging result with high reconstruction accuracy can be achieved with fewer iterations. The flowchart of the hybrid BA is shown in Fig. 2, and the modifications to the original BA is highlighted using bold text.

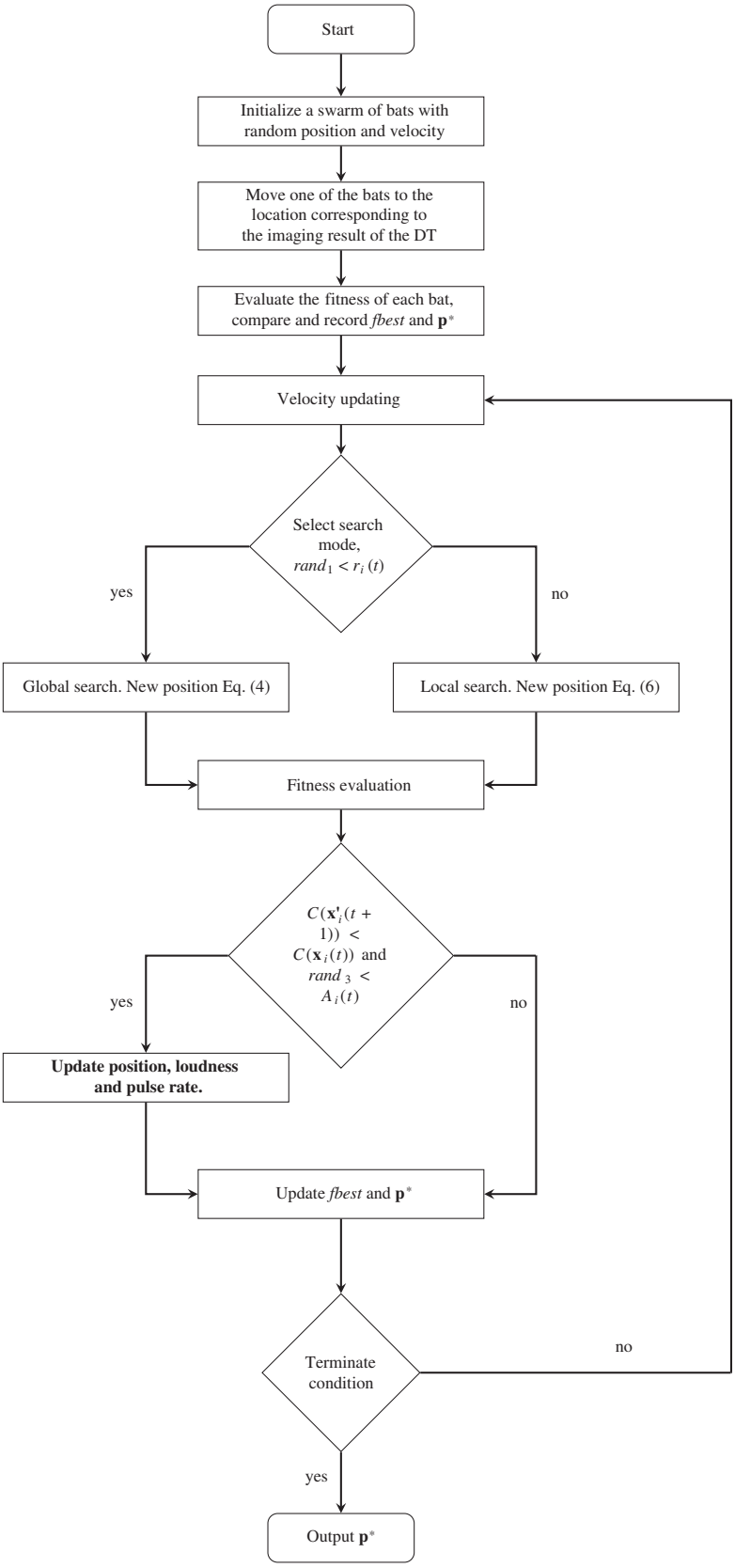

Figure 2. The flow chart of the hybrid BA-based algorithm.

4. NUMERICAL ANALYSIS

In this section, numerical experiments of two-dimensional dielectric scatterers are carried out to assess the effectiveness of the hybrid BA-based inversion algorithm. And the imaging results from the DT and the PSO are presented for comparison. The scattered data are generated using a 2-D integral equation solver with Matlab, and the simulation configuration is shown in Fig. 1. The implementation of DT can be found in [14], and the PSO is implemented according to [26] and [31].

In [31], the PSO is used to reconstruct 2-D dielectric objects, and the optimization results are obtained after 10,000 iterations. On the other hand, in our methods, only a few hundreds of iterations are needed. Therefore, in order to fairly compare the inversion performance of the PSO and BA, diffraction tomographic images are also used as an initial guess of the PSO.

In test 1, the imaging domain is a square area of 60 cm × 60 cm in the free space. The center of the square is set as the origin of the coordinate system. Outside the imaging area, 18 transducers are evenly distributed on a circle with a radius of 2 m and centered at the origin. During the imaging process, each transducer emits 1 GHz TMz waves in turn while all transducers record the scattered field data. This generates a complex matrix of size 18×18 for reconstruction. This exact configuration is an example. The cost function is irrelevant to the distance and frequency. The algorithm should stay valid for different configurations. The imaging domain is evenly divided into $N = 9 \times 9 = 81$ small squares, and it is assumed that permittivity is uniform within each cell.

When setting the parameters in the hybrid BA, we referred to the conclusions of related literatures [38, 40] and made calibrations specifically for the inverse problems in this paper. The result of the calibration is given as follows. The frequency is between 0 and 2; the initial values of loudness $\{A_i(0)|i = 1, 2, \ldots, P\}$ are set to random values between [0, 1]; the pulse emission rate $\{r_i(0)|i = 1, 2, \ldots, P\}$ is randomly initialized within [0, 0.1]; the parameters α in Equation (7) and ξ in Equation (9) are set to 0.99 and 0.9, respectively. Finally, the swarm sizes of the hybrid BA and PSO are both set to 50 (the number of particles is usually between 20 and 60 [41–43]). The control parameters of PSO are set as follows: the cognitive acceleration coefficient and the social acceleration coefficient are both set as 2.0, and the weight coefficient is 0.4 (these settings are consistent with [31]).

The objects to be reconstructed are isolated dielectric points with relative permittivity between 1.4 and 2.0, as shown in Fig. 3(a). The imaging result of the DT is shown in Fig. 3(b), which is a low-pass representation of the original scatterer. The optimization results of the PSO and the hybrid BA after 200 iterations are shown in Figs. 3(c) and (d), respectively. Fig. 4 depicts the convergence trajectory of the cost function value versus the number of iterations in the BA. In order to explicitly compare the real and reconstructed relative permittivity values of each cell, Fig. 5 plots the contrast distribution in a one-dimensional view. Next, to further test the robustness of the algorithm, Gaussian white noises were added to the scattered field data. Three cases, respectively with 20 dB, 10 dB, and 5 dB of signal-to-noise ratio (SNR), are studied, and the corresponding imaging results of the BA-based inversion algorithm are shown in Fig. 6. The corresponding convergence curves are depicted in Fig. 7.

It can be observed from these numerical results that the BA-based inversion algorithm can accurately reconstruct the location and permittivity value of each scattering point even in the presence of strong noise. However, the optimization results of the PSO-based and hybrid BA-based inversions are not notably different. Next, a more complex inversion target is introduced to further verify the effectiveness of the BA-based inversion method and its advantages over other algorithms.

In test 2, the imaging area is expanded to a size of 1 m × 1 m. The target consists of two homogeneous squares with 0.21 m side length. The first square is centered at $(-0.14\,\text{m}, -0.14\,\text{m})$ and has a relative permittivity of $\varepsilon_r = 2.5$. The other one is centered at $(0.07\,\text{m}, 0.07\,\text{m})$ and has a relative permittivity of $\varepsilon_r = 2.0$.

The actual profile, the reconstructed image by DT, and the image by the PSO are shown in Figs. 8(a), (b), and (c), respectively. The reconstructed image by DT is very fuzzy, and the PSO can roughly reconstruct the outline of the target. The results of Figs. 8(d) and (e) are both obtained by BA optimization, and the difference is the updating rule of pulse emission rate. The traditional exponential increasing formula is adopted to generate the image of (d), and the modified decreasing strategy is adopted to generate (e). It can be found that the modified strategy yields a more accurate reconstruction. As seen from the convergence curves in Fig. 9, the PSO appears precocious and falls into a local extremum, while the improved BA has better convergence effect than the traditional BA.

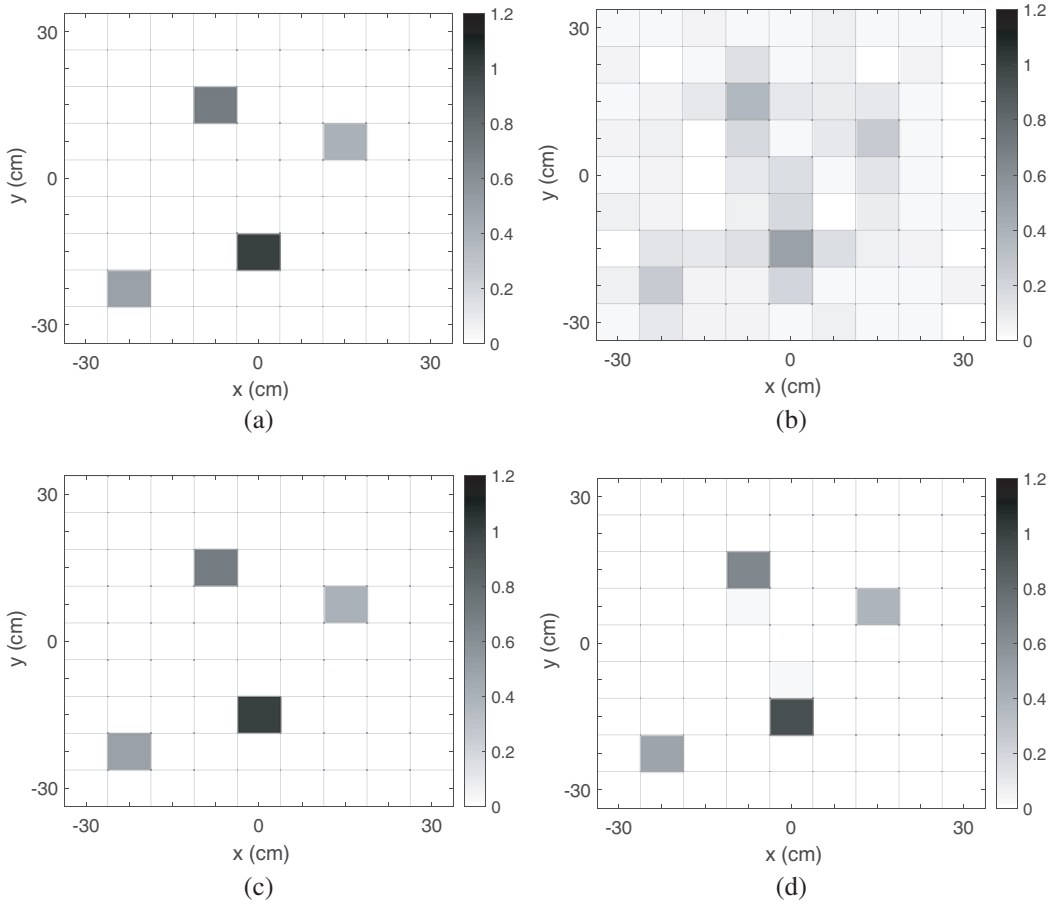

Figure 3. Reconstructed contrast distribution of isolated scatter points. (a) The exact profile. (b) The reconstructed image by the DT. (c) The reconstruction result by the PSO. (d) The reconstruction result by the BA.

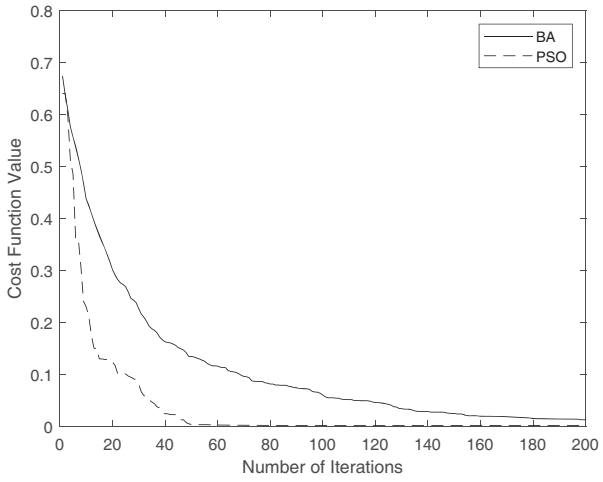

Figure 4. Reconstruction of isolated scatter points. The convergence trajectory of the PSO and the BA.

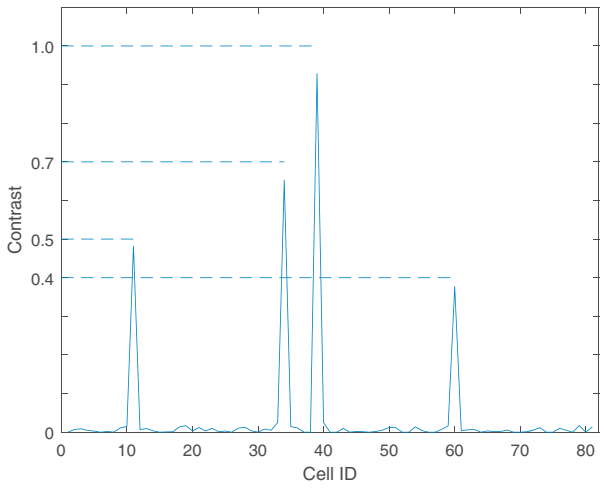

Figure 5. Reconstruction of isolated scatter points. The contrast distribution reconstructed by the proposed algorithm in one-dimensional view.

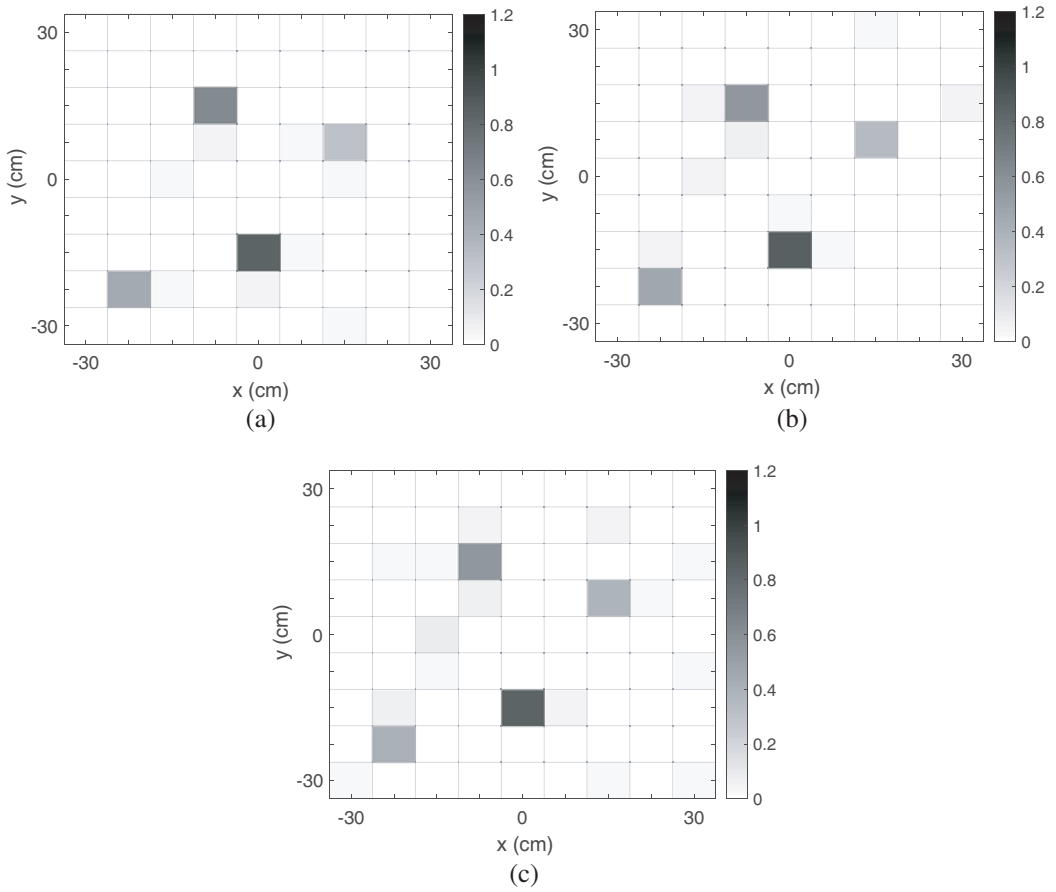

Figure 6. Reconstructed contrast distribution of isolated scatter points with noisy data. Imaging results by the proposed algorithm with SNR: (a) 20 dB, (b) 10 dB and (c) 5 dB.

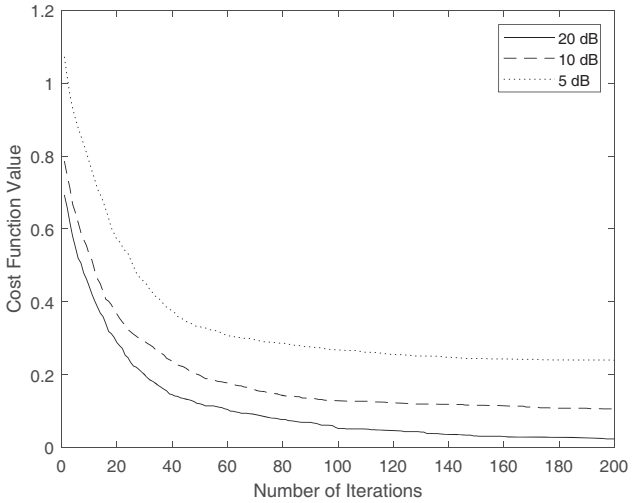

Figure 7. Reconstruction of isolated scatter points with noisy data. The convergence trajectory of the BA.

The reconstruction results with noise contamination are also presented. In Fig. 10, reconstruction results when SNR = 20 dB, 10 dB, and 5 dB are shown by (a), (b), and (c), respectively. It can be observed that the BA-based algorithm is also able to reconstruct complex objects in a noisy environment.

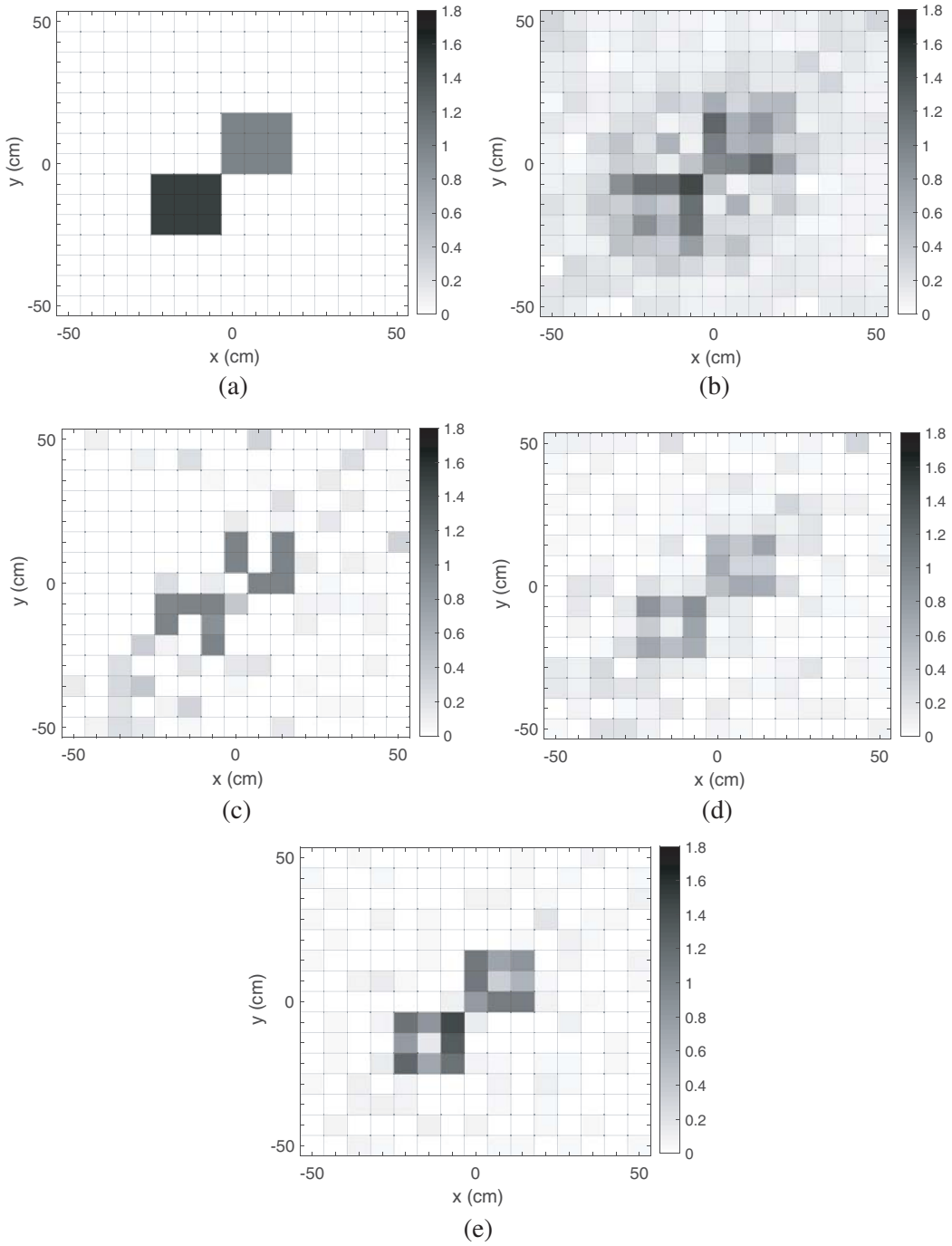

Figure 8. Reconstructed contrast distribution of two homogeneous squares with 0.21 m side length ($\varepsilon_{r1} = 2.5$, $\varepsilon_{r2} = 2.0$). (a) The true objects. (b) The reconstructed image by the DT. (c) The imaging result by the PSO. (d) The image by the conventional BA. (e) The image by the hybrid BA.

In terms of computational efficiency, the BA-based algorithm shares the same complexity as the PSO method. The code is implemented using Matlab and evaluated on a computer using Intel i5-8500u CPU and 16 GB memory. The DT is extremely efficient and takes around 0.001 s and 0.002 s for test 1 and test 2, respectively. The reconstruction test 1 using PSO and BA-based algorithm takes 580.03 s and 659.68 s, respectively. Test 2 takes 11595.00 s and 9114.68 s for PSO and BA-based algorithm respectively. The reason that PSO is more efficient in test 1 is that when the individuals converge to

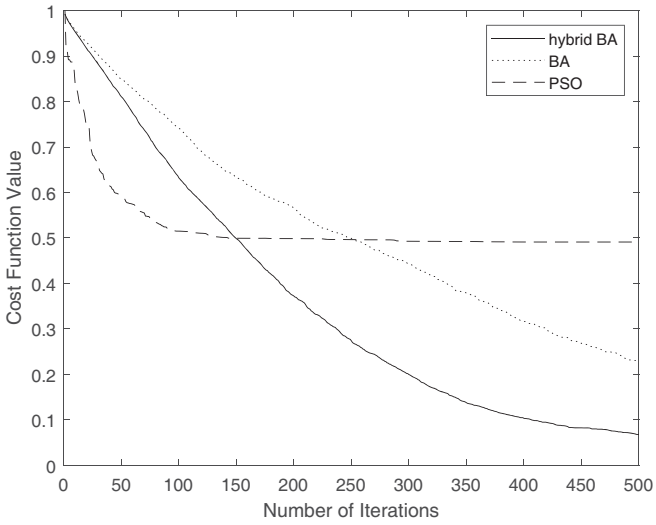

Figure 9. The convergence curves in test 2. The curves correspond to the PSO, the conventional BA, and hybrid BA respectively.

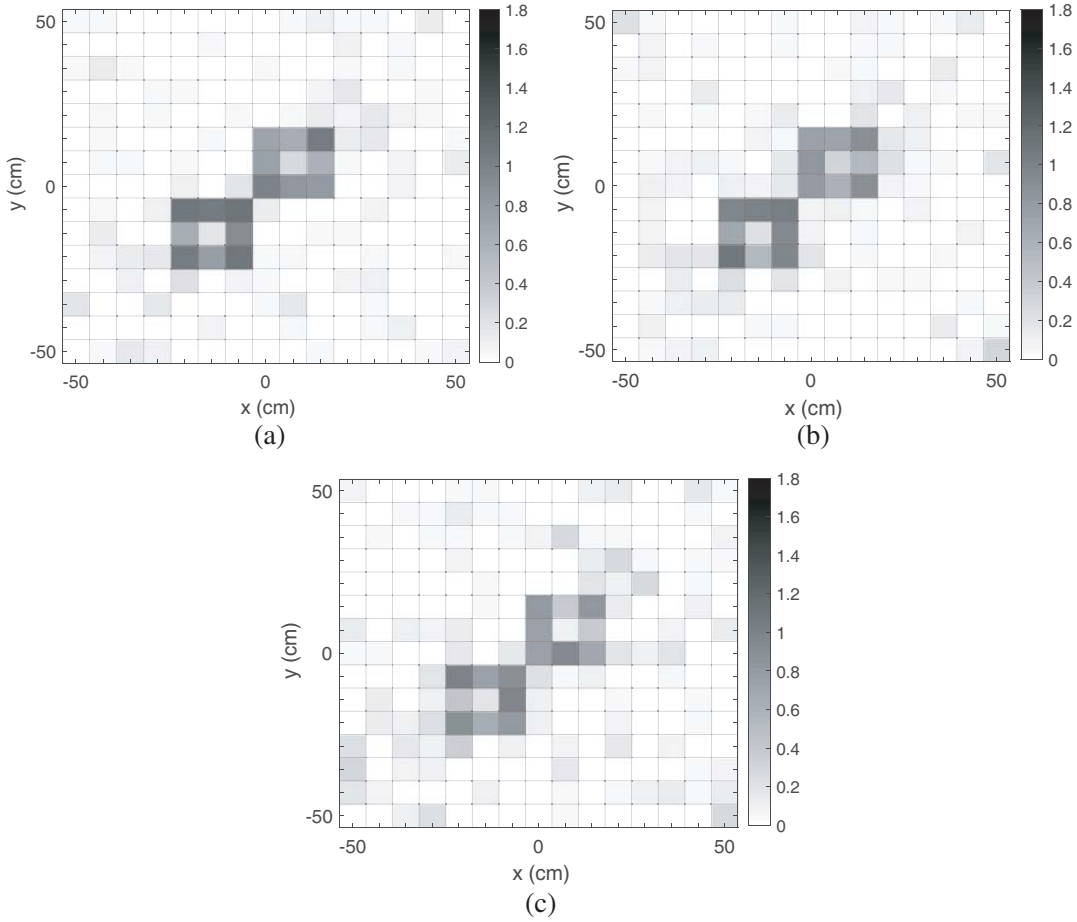

Figure 10. Reconstructed contrast distribution of two square scatterers with noisy data. Imaging results by the proposed algorithm with SNR: (a) 20 dB, (b) 10 dB and (c) 5 dB.

the solution, the corresponding system matrices of forward scattering equation are better-conditioned and thus require fewer iterations to solve. Other than this, the BA-based algorithm and PSO share similar computational complexity.

5. CONCLUSION

In this paper, a hybrid BA-based inversion algorithm is proposed to solve electromagnetic inverse scattering problems. First, an initial image of the scatterer is obtained by the DT. Then a hybrid BA optimization is applied to reconstruct the target with higher accuracy.

In standard BA, the initial position of the individual is generated by random selection in the search space, and it often needs many iterations to find the optimal solution. Since computational efficiency is the bottleneck that blocks the application of stochastic optimization algorithms to electromagnetic inverse problems, we propose a hybrid inversion strategy. It could greatly reduce the number of iterations and combine the efficiency of the linear reconstruction algorithm with the precision of the stochastic optimization algorithm. Moreover, in order to avoid the optimization falling into local minima, the exponential increasing law of pulse emission rate is replaced with a decreasing scheme to improve the global searching ability of the algorithm in the early stage.

The numerical simulation results show that this hybrid BA-based inversion algorithm can effectively reconstruct 2-D dielectric targets, even in the presence of strong noises. And the reconstruction accuracy of complex scatterers is better than that of the DT and PSO. Future research will focus on larger and more complex microwave imaging problems to further test and improve the performance of the inversion algorithm.

ACKNOWLEDGMENT

This work was supported in part by the Shanghai Sailing Program under Grant 18YF1418600 and in part by the National Natural Science Foundation of China under Grant 61801293.

REFERENCES

1. Pastorino, M., *Microwave Imaging*, Vol. 208, John Wiley & Sons, 2010.
2. Colton, D. and R. Kress, *Inverse Acoustic and Electromagnetic Scattering Theory*, Vol. 93, Springer Nature, 2019.
3. Bolomey, J. C., A. Izadnegahdar, L. J. Roca, C. P. Du Mezeray, and G. Peronnet, "Microwave diffraction tomography for biomedical applications," *IEEE Transactions on Microwave Theory and Techniques*, Vol. 30, No. 11, 1998–2000, 1982.
4. Abubakar, A., P. M. Van den Berg, and J. J. Mallorqui, "Imaging of biomedical data using a multiplicative regularized contrast source inversion method," *IEEE Transactions on Microwave Theory and Techniques*, Vol. 50, No. 7, 1761–1771, 2002.
5. Shea, J. D., P. Kosmas, S. C. Hagness, and B. D. Van Veen, "Three-dimensional microwave imaging of realistic numerical breast phantoms via a multiple-frequency inverse scattering technique," *Medical Physics*, Vol. 37, No. 8, 4210–4226, 2010.
6. Lu, Y., J. Zhao, and G. Wang, "Edge-guided dual-modality image reconstruction," *IEEE Access*, Vol. 2, 1359–1363, 2014.
7. Caorsi, S., A. Massa, M. Pastorino, and M. Donelli, "Improved microwave imaging procedure for nondestructive evaluations of two-dimensional structures," *IEEE Transactions on Antennas and Propagation*, Vol. 52, No. 6, 1386–1397, 2004.
8. Almeida, E. R., J. L. Porsani, I. Catapano, G. Gennarelli, and F. Soldovieri, "Microwave tomography-enhanced GPR in forensic surveys: The case study of a tropical environment," *IEEE Journal of Selected Topics in Applied Earth Observations and Remote Sensing*, Vol. 9, No. 1, 115–124, 2015.

9. Goodman, D., "Ground-penetrating radar simulation in engineering and archaeology," *Geophysics*, Vol. 59, No. 2, 224–232, 1994.
10. Frigui, H., L. Zhang, and P. D. Gader, "Context-dependent multisensor fusion and its application to land mine detection," *IEEE Transactions on Geoscience and Remote Sensing*, Vol. 48, No. 6, 2528–2543, 2010.
11. Gurbuz, T. U., B. Aslanyurek, E. P. Karabulut, and I. Akduman, "An efficient nonlinear imaging approach for dielectric objects buried under a rough surface," *IEEE Transactions on Geoscience and Remote Sensing*, Vol. 52, No. 5, 3013–3022, 2013.
12. Chen, G., J. Pei, F. Yang, X. Y. Zhou, Z. Sun, and T. J. Cui, "Terahertz-wave imaging system based on backward wave oscillator," *IEEE Transactions on Terahertz Science and Technology*, Vol. 2, No. 5, 504–512, 2012.
13. Jiang, Y., Y. Qin, H. Wang, B. Deng, K. Liu, and B. Cheng, "A side-lobe suppression method based on coherence factor for terahertz array imaging," *IEEE Access*, Vol. 6, 5584–5588, 2018.
14. Chew, W. C., *Waves and Fields in Inhomogeneous Media*, IEEE Press, 1995.
15. Bleistein, N. and J. K. Cohen, "Nonuniqueness in the inverse source problem in acoustics and electromagnetics," *Journal of Mathematical Physics*, Vol. 18, No. 2, 194–201, 1977.
16. Devaney, A. and G. Sherman, "Nonuniqueness in inverse source and scattering problems," *IEEE Transactions on Antennas and Propagation*, Vol. 30, No. 5, 1034–1037, 1982.
17. Slaney, M., A. C. Kak, and L. E. Larsen, "Limitations of imaging with first-order diffraction tomography," *IEEE Transactions on Microwave Theory and Techniques*, Vol. 32, No. 8, 860–874, 1984.
18. Habashy, T. M. and A. Abubakar, "A general framework for constraint minimization for the inversion of electromagnetic measurements," *Progress In Electromagnetics Research*, Vol. 46, 265–312, 2004.
19. Shah, P., U. K. Khankhoje, and M. Moghaddam, "Inverse scattering using a joint l_1–l_2 norm-based regularization," *IEEE Transactions on Antennas and Propagation*, Vol. 64, No. 4, 1373–1384, 2016.
20. De Zaeytijd, J., A. Franchois, and J.-M. Geffrin, "A new value picking regularization strategyapplication to the 3-d electromagnetic inverse scattering problem," *IEEE Transactions on Antennas and Propagation*, Vol. 57, No. 4, 1133–1149, 2009.
21. Van Den Berg, P. M. and R. E. Kleinman, "A contrast source inversion method," *Inverse Problems*, Vol. 13, No. 6, 1607, 1997.
22. Chen, X., "Application of signal-subspace and optimization methods in reconstructing extended scatterers," *Journal of the Optical Society of America A*, Vol. 26, No. 4, 1022–1026, 2009.
23. Chen, X., "Subspace-based optimization method for solving inverse-scattering problems," *IEEE Transactions on Geoscience and Remote Sensing*, Vol. 48, No. 1, 42–49, 2009.
24. Wang, Y. and W. C. Chew, "An iterative solution of the two-dimensional electromagnetic inverse scattering problem," *International Journal of Imaging Systems and Technology*, Vol. 1, No. 1, 100–108, 1989.
25. Donelli, M., D. Franceschini, A. Massa, M. Pastorino, and A. Zanetti, "Multi-resolution iterative inversion of real inhomogeneous targets," *Inverse Problems*, Vol. 21, No. 6, S51, 2005.
26. Kennedy, J., "Swarm intelligence," *Handbook of Nature-inspired and Innovative Computing*, 187–219, Springer, 2006.
27. Engelbrecht, A. P., *Fundamentals of Computational Swarm Intelligence*, John Wiley & Sons, Ltd., Hoboken, 2005.
28. Rocca, P. M. B., M. Donelli, D. Franceschini, and A. Massa, "Evolutionary optimization as applied to inverse scattering problems," *Inverse Problems*, Vol. 25, No. 12, 123003, 2009.
29. Rocca, P., G. Oliveri, and A. Massa, "Differential evolution as applied to electromagnetics," *IEEE Antennas and Propagation Magazine*, Vol. 53, No. 1, 38–49, 2011.
30. Salucci, M., L. Poli, N. Anselmi, and A. Massa, "Multifrequency particle swarm optimization for enhanced multiresolution GPR microwave imaging," *IEEE Transactions on Geoscience and Remote Sensing*, Vol. 55, No. 3, 1305–1317, 2016.

31. Donelli, M. and A. Massa, "Computational approach based on a particle swarm optimizer for microwave imaging of two-dimensional dielectric scatterers," *IEEE Transactions on Microwave Theory and Techniques*, Vol. 53, No. 5, 1761–1776, 2005.
32. Caorsi, S., M. Donelli, A. Lommi, and A. Massa, "Location and imaging of two-dimensional scatterers by using a particle swarm algorithm," *Journal of Electromagnetic Waves and Applications*, Vol. 18, No. 4, 481–494, 2004.
33. Yang, X.-S. and A. H. Gandomi, "Bat algorithm: A novel approach for global engineering optimization," *Engineering Computations*, Vol. 29, No. 5, 464–483, 2012.
34. Hasançebi, O., T. Teke, and O. Pekcan, "A bat-inspired algorithm for structural optimization," *Computers & Structures*, Vol. 128, 77–90, 2013.
35. Sabba, S. and S. Chikhi, "A discrete binary version of bat algorithm for multidimensional knapsack problem," *International Journal of Bio-inspired Computation*, Vol. 6, No. 2, 140–152, 2014.
36. Cai, X., L. Wang, Q. Kang, and Q. Wu, "Adaptive bat algorithm for coverage of wireless sensor network," *International Journal of Wireless and Mobile Computing*, Vol. 8, No. 3, 271–276, 2015.
37. Cui, Z., F. Li, and Q. Kang, "Bat algorithm with inertia weight," *Chinese Automation Congress*, 792–796, 2015.
38. Yang, X.-S. and X. He, "Bat algorithm: Literature review and applications," *International Journal of Bio-inspired Computation*, Vol. 5, No. 3, 141–149, 2013.
39. Cai, X., W. Li, Q. Kang, L. Wang, and Q. Wu, "Bat algorithm with oscillation element," *International Journal of Innovative Computing and Applications*, Vol. 6, Nos. 3–4, 171–180, 2015.
40. Xue, F., Y. Cai, Y. Cao, Z. Cui, and F. Li, "Optimal parameter settings for bat algorithm," *International Journal of Bio-Inspired Computation*, Vol. 7, No. 2, 125–128, 2015.
41. Bergh, F. V. D. and A. P. Engelbrecht, "Effects of swarm size on cooperative particle swarm optimisers," *Proceedings of the 3rd Annual Conference on Genetic and Evolutionary Computation*, 892–899, 2001.
42. Shi, Y. and R. C. Eberhart, "Empirical study of particle swarm optimization," *Proceedings of the 1999 Congress on Evolutionary Computation-CEC99 (Cat. No. 99TH8406)*, Vol. 3, 1945–1950, IEEE, 1999.
43. Dozier, G. and A. Carlisle, "An off-the-shelf PSO," *Proc. of the Particle Swarm Optimization Workshop*, 1–6, 2001.